Thresholds of flow-induced bed disturbances and their effects on stream metabolism in an agricultural river

Ben L. O'Connor,[1] Judson W. Harvey,[2] and Lauren E. McPhillips[3]

Received 6 October 2011; revised 20 May 2012; accepted 6 June 2012; published 4 August 2012.

[1] Storm-driven flow pulses in rivers destroy and restructure sediment habitats that affect stream metabolism. This study examined thresholds of bed disturbances that affected patch- and reach-scale sediment conditions and metabolism rates. A 4 year record of discharge and diel changes in dissolved oxygen concentrations (ΔDO) was analyzed for disturbances and recovery periods of the ΔDO signal. Disturbances to the ΔDO signal were associated with flow pulses, and the recovery times for the ΔDO signal were found to be in two categories: less than 5 days (30% of the disturbances) or greater than 15 days (70% of the disturbances). A field study was performed during the fall of 2007, which included a storm event that increased discharge from 3.1 to 6.9 m^3/s over a 7 h period. During stable flow conditions before the storm, variability in patch-scale stream metabolism values were associated with sediment texture classes with values ranging from -16.4 to 2.3 g $O_2/m^2/d$ (negative sign indicates net respiration) that bounded the reach-averaged rate of -5.6 g $O_2/m^2/d$. Hydraulic modeling of bed shear stresses demonstrated a storm-induced flow pulse mobilized approximately 25% of the bed and reach-scale metabolism rates shifted from -5 to -40 g $O_2/m^2/d$. These results suggest that storm-induced bed disturbances led to threshold behavior with respect to stream metabolism. Small flow pulses resulted in partial-bed mobilization that disrupted stream metabolism by increased turbidity with short recovery times. Large flow pulses resulted in full-bed mobilization that disrupted stream metabolism by destroying periphyton habitats with long recovery times.

Citation: O'Connor, B. L., J. W. Harvey, and L. E. McPhillips (2012), Thresholds of flow-induced bed disturbances and their effects on stream metabolism in an agricultural river, *Water Resour. Res.*, *48*, W08504, doi:10.1029/2011WR011488.

1. Introduction

[2] Floods play an important role in regulating river ecosystems by controlling spatial and temporal patterns of biota and ecological processes [*Junk et al.*, 1989; *Biggs et al.*, 1999]. Stream metabolism measures primary production and respiration, which incorporate ecological processes such as the generation of biomass, along with nutrient and organic matter cycling in river ecosystems [e.g., *Mulholland et al.*, 2001; *Fellows et al.*, 2006]. Fluvial processes affect stream metabolism through physical interactions with biota and by geomorphic processes that generate a mosaic of habitat conditions [*Cardinale et al.*, 2002; *Warnaars et al.*, 2007; *Munn et al.*, 2010]. Thus, stream metabolism is a highly integrative measure of ecological processes that reflects the overall health of a river, and it is a metric that is sensitive to physical habitat characteristics and disturbances relating to floods and land use practices within a watershed [e.g., *Houser et al.*, 2005; *Izagirre et al.*, 2008].

[3] Differences in stream metabolism rates among small streams spanning a wide range of watershed characteristics have shown that the primary controllers of stream metabolism are light availability (canopy cover and turbidity) and nutrients (primarily phosphorus) [e.g., *Mulholland et al.*, 2001; *Izagirre et al.*, 2008]. For agricultural watersheds, it has been shown that physical habitat, light availability, and fluvial processes (including shear stresses, water depths, and turbidity) are better than biomass measures or nutrient enrichment factors at explaining variability in stream metabolism rates [*Morgan et al.*, 2006; *Frankforter et al.*, 2010]. Alterations to the landscape in agricultural watersheds typically result in rivers with limited riparian shading, shallow depths, excess nutrients, seasonally warm temperatures, dense algal assemblages, and an abundance of fine sediments with all of these habitat-related factors having the ability to enhance stream metabolism rates [*Wiley et al.*, 1990; *Young and Huryn*, 1999]. The importance of fluvial processes with respect to stream metabolism in agricultural rivers is considered to be the combination of flashy hydrology and unstable sediment beds, which have the potential to make physical habitat conditions both spatially and temporally dynamic [*Atkinson et al.*, 2008],

[1]Environmental Science Division, Argonne National Laboratory, Argonne, Illinois, USA.
[2]National Research Program, U.S. Geological Survey, Reston, Virginia, USA.
[3]Department of Biological and Environmental Engineering, Cornell University, Ithaca, New York, USA.

Corresponding author: B. L. O'Connor, Argonne National Laboratory, 9700 S. Cass Ave., EVS Bldg. 240, Argonne, IL 60439, USA. (boconnor@anl.gov)

This paper is not subject to U.S. copyright.
Published in 2012 by the American Geophysical Union.

and decrease light availability through increased turbidity [*Morgan et al.*, 2006].

[4] The response of stream metabolism to floods relates directly to ecosystem stability factors described by resistance and resilience [*Uehlinger*, 2000; *Folke et al.*, 2004]. Periphyton that carry out critical biogeochemical processes in rivers are primarily attached to, or embedded within, the sediment bed [*Brunke and Gonser*, 1997; *Giller and Malmqvist*, 2002]. In addition, aquatic vegetation contains substantial epiphyton communities that can be entrained at high flows [*Harvey et al.*, 2011]. Floods generate additional shear stress that affects periphyton and epiphyton attachment, as well as the incipient motion of sediment particles resulting in increased turbidity and the reorganization of physical habitats. Small-scale heterogeneity in hydraulic conditions can regulate biogeochemical processes and community structure of benthic microorganisms and biofilms under steady flow conditions between floods [e.g., *Arnon et al.*, 2007; *O'Connor and Hondzo*, 2008; *Singer et al.*, 2010]. Thus, ecosystem resistance relates to physical conditions that allow for habitats and biological communities to withstand flood-induced shear stresses, whereas ecosystem resilience relates to fluvial and biological processes that affect the recovery of habitats and their associated biological communities after a flood event.

[5] Conceptual models and field studies relating stream metabolism to floods have primarily focused on events that mobilize the entire sediment bed [*Young and Huryn*, 1996; *Uehlinger and Naegeli*, 1998; *Biggs et al.*, 1999;*Uehlinger*, 2000, 2006; *Cronin et al.*, 2007; *Atkinson et al.*, 2008]. All of these studies examined stream metabolism and flooding at the watershed and reach scales, which do not take into account subreach variability in physical habitat characteristics or patch-scale photosynthesis and respiration rates. Heterogeneity in sediment substrata has been shown to increase patch-scale rates of primary productivity and respiration [*Cardinale et al.*, 2002], as well as increase the depth of oxic sediment zones [*Wilson and Dodds*, 2009]. In addition, at patch to reach scales, benthic algae is regulated by variability in physical habitat characteristics, with higher biomass typically associated with sediments consisting of coarser sand to cobble particle sizes [*Munn et al.*, 2010; *Ogdahl et al.*, 2010].

[6] The connection between biotic communities with sediment substrata suggests that quantifying physical habitat conditions relating to stream metabolism should incorporate properties of the streambed, and sediment characteristics have been shown to have a high degree of spatial organization in rivers [*Paola and Seal*, 1995; *Crowder and Diplas*, 1997; *Dietrich et al.*, 2006]. Gravel- and sand-bedded rivers can be grouped into sediment textural patches (similar particle sizes and sorting) that originate from variability in hydraulics and channel characteristics causing preferential areas of entrainment and deposition [*Buffington and Montgomery*, 1999]. These sediment texture patches can also be categorized as free, fixed, or forced with respect to hydraulic and geomorphic processes that allow for sediment transport (free), are immobilized by local coarsening (fixed), and that are created by topographic features such as bars (forced) [*Nelson et al.*, 2009]. When characterizing physical habitat according to sediment texture patches, it is important to consider the fluvial and geomorphic processes controlling the generation of free, fixed, and forced sediment patches, as these processes dictate how various streambed habitats are disturbed by various levels of flooding.

[7] In this study, we examined the effects of storm-induced flow pulses (varying levels of flooding events) on stream metabolism rates, and quantify threshold behavior in the mobilization of sediment texture patches at the subreach scale that regulates the response of stream metabolism in an agricultural river. The study approach was twofold with an examination of the long-term temporal variability of discharge and dissolved oxygen data, along with a field-based examination of the subreach scale response in hydraulics, sediment texture, and stream metabolism rates to a single flood event. Discharge and water quality gage data were used to assess stream metabolism responses to flow pulses from 2005 to 2008. Field measurements of patch- and reach-scale metabolism measurements, sediment texture (including algae and benthic organic matter coverages), and bathymetry were used in combination with a hydraulic model to assess stream metabolism variability at the subreach scale and in relation to a flood event. Given the importance of subreach variability in physical habitat on stream metabolism, we hypothesized that flow disturbance effects on stream metabolism would vary according to the response of various sediment texture patches to flooding. Specifically, we examined whether a flood that mobilizes only a portion of the streambed would affect stream metabolism by decreasing light availability because of turbidity, by the disturbance to periphyton communities because of sediment scouring, or by a combination of these effects.

2. Site Description and Study Design

[8] This study was conducted within the Eastern Iowa Basins study unit of the National Water-Quality Assessment Program (U.S. Geological Survey, USGS). This region is within the Des Moines Lobe landform region, characterized by low relief with rolling hillsides and is composed of poorly drained glacial till surface materials with alluvium along streams [*Kalkhoff et al.*, 2000]. Historically, this region contained shallow ponds and wetlands, but extensive ditching in the early 1900s was done to improve drainage and allow for agricultural production, resulting in a system of several first-order streams that feed the few larger river reaches in the region. Annual precipitation averages 76 cm (1951–1980), most of which occurs between April and October each year [*Becher et al.*, 2001]. Runoff is primarily conveyed as overland flow except in areas that are tile-drained, and streams are supplied by runoff and groundwater discharge [*Kalkhoff et al.*, 2000]. Water quality impairments include high nutrient and pesticide concentrations [*Schnoebelen et al.*, 2003; *Tomer et al.*, 2008] with biological communities (fish, algal, and macroinvertebrate) composed of species tolerant to environmental degradation [*Kalkhoff et al.*, 2000].

[9] The study reach was located on the South Fork Iowa River approximately 1.2 km upstream of USGS streamflow gaging station 05451210 (42°18′N54″, 93°09′W08″, Figure 1a). The contributing drainage area to the gaging station is 580 km^2, of which 95% is used to support row crop agriculture and large-scale animal feed operations [*Karlen et al.*, 2008]. The study reach was 185 m in length with geomorphic features that include a meander bend upstream of the reach and an island bar separating the upstream 90 m

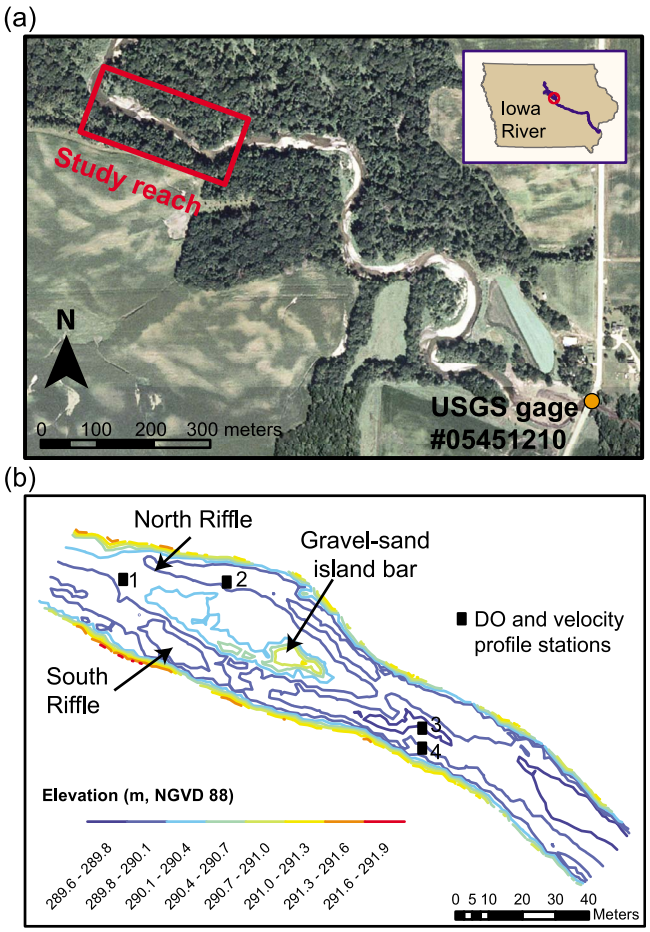

Figure 1. The South Fork Iowa River study reach: (a) aerial photograph and (b) measured bathymetry, stream bank topography, and measurement locations of dissolved oxygen concentration and velocity profiles.

into two channels (Figures 1a and 1b). Habitat characteristics of the study reach include an average riparian zone width of 32 m (with a riparian tree density of 43%), an open canopy (107°, with 9% shading), and predominately sand and gravel streambed sediments [*Sorenson et al.*, 1999].

[10] The study design was twofold, consisting of (1) an examination of discharge and dissolved oxygen data collected at the gaging station and (2) a field-based examination of reach- and patch-scale measures of physical habitat and stream metabolism. The goal of the first approach was to identify the characteristics of flooding events and recovery periods that disrupt and reestablish the steady flow patterns of stream metabolism, respectively. This analysis used spring, summer, and fall measurements of discharge, dissolved oxygen, and meteorological conditions collected from 2005 to 2008. In 2005 and 2006, total annual precipitation was on the order of the long-term mean. In 2007 and 2008, total annual precipitation was well above the long-term mean, coinciding with the record floods that occurred in 2008 throughout central Iowa [*Buchmiller and Eash*, 2010]. The second approach involved a detailed characterization of a study reach performed from 26 September 2007 to 4 October 2007. This site characterization focused on measurements of sediment substrata, bathymetry, and hydraulics, in order to define physical habitat patches and relate those to patch- and reach-scale stream metabolism measurements. A large frontal system passed over Iowa on 2 October 2007, which delivered 5 cm of rainfall over a 7 h period to the study area. The storm event resulted in a near doubling of the discharge in the South Fork Iowa River at the study reach, which resulted in substantial sediment transport and partial inundation of the island bar (Figure 2). A hydraulic model was developed to examine the effects of this flooding event on the physical habitat patches and relate those to the measured stream metabolism rates.

3. Methods

3.1. Time Series Analysis of Discharge and Dissolved Oxygen Data

[11] The effects of storm events and resulting flow pulses on stream metabolism were analyzed using stream gage (USGS, 05451210) and meteorological station (USGS, 421852093091202) data collected near the study reach from 2005 to 2008. For each year, there was little lag time (typically 1–4 days) between precipitation events and peaks in discharge and there was a high degree of seasonality in the

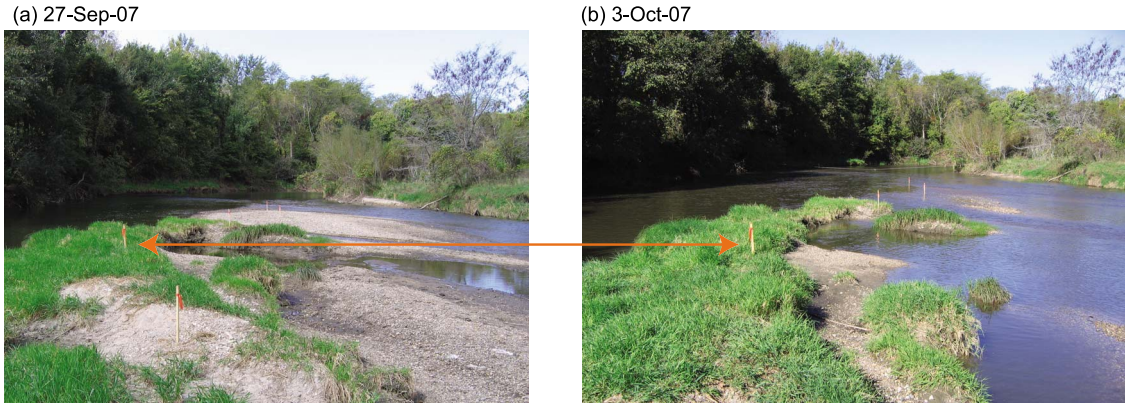

Figure 2. Photograph looking upstream from the study reach's island bar (a) on 27 September 2007 under preflood conditions (Q = 3.1 m^3/s) and (b) on 3 October 2007 under postflood conditions (Q = 6.9 m^3/s). The arrow shows the location of the same survey stake in each photo.

flow patterns (Figure S1 in the auxiliary material).[1] There are numerous ways to quantify temporal variability in flows (see *Olden and Poff* [2003] for an overview of flow variability metrics). The intent for this study was to examine correlations between peaks in the flow hydrograph to disruptions in the stream metabolism signal. Several methods were considered for quantifying flow pulses, and it was determined that increases in daily averaged discharge values greater than 25% were the most efficient way to capture the observable peaks in the annual hydrographs.

[12] Dissolved oxygen concentrations were measured from April through October from 2005 to 2008 at the stream gage (USGS, 05451210). Several data gaps in the dissolved oxygen record were the result of sensor damage and calibration drift. These data gaps include 1–4 April, 2–14 June, and 12–19 July in 2005; 1–20 April and 13–18 September in 2006; 1–5 April, 24 April to 14 June, and 24–31 October in 2007; and 1–16 April in 2008. In agricultural rivers, the combination of high nutrient loadings and low shading enhances biological productivity, which produces large diel changes in dissolved oxygen concentrations [e.g., *Morgan et al.*, 2006]. The difference between the daily minimum and maximum dissolved oxygen concentration (ΔDO) was used as a surrogate measure of stream metabolism in order to characterize the strong diel dissolved oxygen concentration signal. This approach does not account directly for temperature and reaeration effects to stream metabolism measurement, but the use of the diel dissolved oxygen signal has been shown to be a useful indicator of stream metabolism for comparing small streams with varying watershed impairments [*Mulholland et al.*, 2005]. Disturbances to the ΔDO signal were identified as values falling below a threshold value. Threshold ΔDO values of 1.5 and 2 mg/L were qualitatively determined by examining the ΔDO signal and discharge record over the entire study period. Corresponding recovery periods were identified as the time periods from initial disturbance to when the ΔDO value went above the threshold value.

3.2. Field-Based Physical Habitat Characterization and Stream Metabolism

[13] Reach and subreach variability in physical habitat characteristics, stream metabolism, and the resulting effects of the 2 October 2007 storm event were assessed using a variety of techniques. Physical habitat was characterized by sediment texture (based on particle sizes and sorting, along with measures of benthic algae and organic material) and bathymetry. The river hydraulics (velocity, flow, and bed shear stress) were quantified using acoustic Doppler velocimeter (ADV) technology, along with the development of a two-dimensional (2-D) hydraulic model of the study reach. Reach-scale stream metabolism was measured using a mass balance of dissolved oxygen approach, which used diel dissolved oxygen concentrations, reach-averaged channel characteristics, and an empirical expression for reaeration. Patch-scale stream metabolism was measured using dissolved oxygen profiles in the sediments in combination with a reactive transport model, which required information on bed shear stress and the hydraulic conductivity to estimate an effective diffusion transport parameter.

[1]Auxiliary materials are available in the HTML. doi:10.1029/2011WR011488.

3.2.1. Sediment Texture and Bathymetry

[14] An initial grid-based, visual survey of the study reach was done in order to identify patches according to sediment texture in a similar fashion as described by *Buffington and Montgomery* [1999]. A measurement grid with a total area of 900 cm^2 and 6 cm $\times$ 6 cm divisions was placed on the streambed at 2 m intervals across the width of stream transects located at 10 m intervals along the length of the study reach. Additional grid measurements were conducted at locations where there were noticeable transitions of bed sediment material or flow conditions between stream transects. The measurement grid was used to estimate the top three sediment particle size classes, as well as the percent coverages of green algae and benthic organic material. A digital camera in a waterproof case was used to photograph grid measurements.

[15] The top three particle size classes were noted at each grid measurement according to the level I classification scheme presented by *Buffington and Montgomery* [1999], which includes silt (Z, nonvisible grains), sand (S, 0.06 to 2 mm), gravel (G, 2 to 60 mm), cobble (C, 60 to 260 mm), and boulders (B, >260 mm). The sediment texture measurements were classified according to the third-second-first most abundant particle size classes at a given location, with the third and second most abundant classes being denoted by a lower case letter and the most abundant class being denoted by a capital letter. For example, a grid measurement that consisted of 65% sand, 20% gravel, and 10% cobble would be labeled as cgS. Any size class that represented less than 5% of the total area was considered negligible, and it was possible to have sediment texture classes consisting of only one or two classes. The spatial arrangement of sediment texture measurements were then examined in order to group measurements of similar sediment texture into larger patches [*Buffington and Montgomery*, 1999].

[16] In addition to sediment texture, estimates of particle sizes d_{50} and d_{90} (particle size for which 50% and 90% of sediment is finer than, respectively) were made using the grid-based measurements. The d_{90} values were estimated visually, representing the larger particle sizes found for each grid measurement. The d_{50} values were estimated according to the most abundant particle size (capital letter in sediment texture classification), and were further classified according to the level II classification scheme presented by *Buffington and Montgomery* [1999]. The use of visual mapping techniques for characterizing sediments allows for larger data coverage with reduced sampling effort, but estimated particle sizes tend to be biased low, and fines are difficult to distinguish [*Bunte and Abt*, 2001]. Visual-based estimates of particle size statistics d_{50} and d_{90} have been shown to have associated errors on the order of 15% and 11%, respectively [*Latulippe et al.*, 2001]. The amount of green algae on the streambed was estimated as the aerial coverage of filamentous green algae identified by the grid measurements. Benthic organic material was classified as either fine (FBOM) or coarse (CBOM), depending upon whether it was predominantly floc material or leaf litter, and coarse woody debris (CWB) was also mapped along the stream reach.

[17] The stream channel bathymetry and bank topography measurements were made using a survey-grade, ProMark2 (Magellan, Santa Clara, California) real-time global positioning system (GPS) operated in static mode with a horizontal accuracy of $\pm$0.012 m and a vertical accuracy of

±0.015 m. Stream bank elevations along with water surface elevation measurements were made at transects located every 10 m along the reach, as well as at several locations between transects to characterize major bed form features, which resulted in an approximate average density of 1 survey point per 10 m^2.

3.2.2. Hydraulic Measurements and Modeling

[18] A FlowTracker ADV (Sontek-YSI, San Diego, California) was used to measure average velocities along stream transects and discharge (Q) measurements were calculated using velocity profiles measured at the downstream cross section according to the velocity-area method [*Turnipseed and Sauer*, 2010]. More detailed velocity profiles were made using a 10 MHz ADV (Sontek-YSI, San Diego, California). Velocity profile measurements were made at depth intervals ranging from 1 to 3 cm (1 cm resolution near the sediments). At each depth, the streamwise, transverse, and vertical velocity components were measured at a sampling frequency of 25 Hz for a duration of 2.5 min.

[19] A 2-D hydraulic model was developed using the FaSTMECH computational code in combination with the USGS Multidimensional Surface water Modeling System (MD_SWMS, http://wwwbrr.cr.usgs.gov/projects/GEOMORPH_Lab/project-MDSWMS.html) in order to stimualte water surface elevations, depth-averaged velocities (streamwise and transverse directions), and bed shear stress throughout the study reach. The FaST-MECH model solves the vertically averaged equations of motion using an orthogonal, curvilinear grid where the flow is assumed to be steady, hydrostatic, and turbulence is accounted for by Reynolds averaging using a eddy viscosity closure. Bed shear stress (τ_b) is calculated using a drag coefficient (C_d) closure for roughness

$$\tau_b = \rho C_d \left(u^2 + v^2\right) \tag{1}$$

where ρ is the water density, u is the streamwise velocity component, and v is the transverse velocity component. The numerical solution scheme used by the FaSTMECH model iteratively solves for velocities and water surface elevations at model nodes until conditions are met regarding the conservation of mass and momentum over the model reach. A more thorough description of the FaSTMECH model is described by *Nelson et al.* [2003] and *McDonald et al.* [2010].

[20] The curvilinear grid for the modeled study reach had an approximate cell size of 1.47 m in the streamwise and transverse directions. GPS survey data of the river bathymetry was mapped to the model grid using the template algorithm in MD_SWMS. Roughness was represented using information from the sediment texture survey, where estimates of d_{90} values were used to calculate roughness length values (z_o = constant · d_{90}). C_d in equation (1) was calculated assuming that the velocity profile in the vertical direction was logarithmic

$$C_d = \left(\frac{1}{\kappa}\left[\ln\left(\frac{h}{z_o}\right) - 1\right]\right)^{-2} \tag{2}$$

where h is the local water depth and κ is the von Kármán constant equal to 0.41. Boundary conditions needed for the FaSTMECH model include Q and downstream water surface elevation. The storm event was modeled using stage and discharge values recorded every 30 min using a stepwise steady state approach over the duration of the storm. The hydraulic model was calibrated to water surface elevations by varying roughness conditions through iterations of the constant term in equating z_o using d_{90} values resulting in $z_o = 0.1 \cdot d_{90}$. Calibration to water surface elevations was done extensively during the steady discharge conditions (3.3 to 3.6 m^3/s) that occurred during the reach characterization and at postflood discharge conditions (6.8 m^3/s). These prestorm and poststorm measurements of water surface elevation and discharge were compared to values measured at the USGS stream gage in order to estimate a stage-discharge relationship for the study reach. The hydraulic model was validated for prestormflow conditions where the average difference between measured and modeled water surface elevations was ±0.013 m.

[21] Flow disturbances to sediment texture patches were assessed using computed Shields stress values

$$\tau^* = \frac{\tau_b}{R_p g d_{50}} \tag{3}$$

where $R_p = \rho_s - \rho$ is the submerged specific gravity of sediment (ρ_s is the sediment density assumed to be 2.65 g/cm^3) and g is the acceleration due to gravity. The threshold for bed movement for the sediment patches was judged to be when τ^* exceeded a critical Shields stress (τ_c^*). For sediment beds of mixed particle sizes, τ_c^* is influenced by the distribution of particle sizes and irregular particle geometries, as well as turbulent fluctuations in bed shear stress such that τ_c^* values have been reported to range from 0.030 to 0.073 in gravel bed rivers [*Buffington and Montgomery*, 1997]. In this study, two values of τ_c^* were considered, 0.03 [*Buffington and Montgomery*, 1997] and 0.0495 [*Wong and Parker*, 2006], in order to represent a low- and high-end estimate of τ_c^* for a river with predominately sand and gravel sediments.

[22] A measure of surface water-groundwater exchange was needed for the analysis of patch-scale metabolism rates (described below), and was assessed using point measurements of hydraulic conductivity and the calculation of an effective diffusion coefficient (hyporheic exchange potential) using data from the hydraulic model. Hydraulic conductivity measurements were performed at select locations along stream transects in order to characterize the identified sediment texture patches. A 10.2 cm diameter plastic tube was inserted into the streambed to a depth of 10 cm (±2 cm depending upon the sediment material), and hydraulic conductivity was measured according to the falling-head method using Hvorslev equation [*Landon et al.*, 2001]. The effective diffusion coefficient D_e was calculated using the scaling expression described by *O'Connor and Harvey* [2008].

3.2.3. Reach- and Patch-Scale Metabolism

[23] Reach-scale metabolism measurements were made using diel dissolved oxygen concentrations as suggested by *Odum* [1956]. The primary processes affecting dissolved oxygen concentrations in a river include transport, photosynthesis, respiration, and reaeration, and the resulting mass balance is typically expressed as

$$\mathrm{NEP} = \mathrm{GPP} - \mathrm{CR} \tag{4}$$

where NEP is the net ecosystem production, GPP is the gross primary productivity, and CR is the community

respiration. The balance of processes affecting dissolved oxygen production, uptake, and exchange allows for a direct calculation of NEP, whereas values of GPP and CR are estimated assuming that GPP is negligible during the night and that daytime values of CR follow a linear regression between predawn and postdusk values [*Marzolf et al.*, 1994].

[24] For the detailed reach study, a two-station mass balance of dissolved oxygen was performed using the automated algorithm presented by *Bales and Nardi* [2007]. Dissolved oxygen, temperature, conductivity, and pH values were recorded at 5 min intervals using YSI 600XLM water quality sondes (Sontek-YSI, San Diego, California). Reach characteristics were derived from the GPS survey and included the reach-averaged bed slope (S), wetted width (B), and depth (H). Information on Q, average velocity (U), and reach travel time (T) were made using a combination of hydraulic measurements and modeling described previously. The reaeration coefficient (K_2) was estimated using the regression equation

$$K_2(1/d) = 1740S^{0.79}U^{0.46}H^{-0.74} \tag{5}$$

which was derived from a set of 315 gas tracer measurements that included a wide variety of stream types [*Moog and Jirka*, 1998].

[25] Patch-scale metabolism measurements were made using dissolved oxygen concentration profiles measured using a needle Clark-type sensor (Unisense, Aarhus, Denmark), which has a sensitivity of 0.1 mg/L and a vertical spatial resolution of 1 mm. The dissolved oxygen needle sensor was traversed through the water column and the near surface sediments using a fitted point gage with a calibrated dial positioning system (Rickly Hydrological, Columbus, Ohio) attached to a tripod stand. The conceptual model used to calculate patch-scale metabolism rates combines processes producing (photosynthesis) and consuming (biological respiration, chemical oxidation, and organic matter decomposition) dissolved oxygen that occur across the sediment-water interface. Estimates of the net volumetric production of dissolved oxygen were obtained by fitting the measured dissolved oxygen profile to the reactive transport equation

$$D_e \frac{d^2C}{dy^2} = P - R \tag{6}$$

where C is the dissolved oxygen concentration, y is the depth into the sediments, D_e is the effective diffusion coefficient described by equation (35) of *O'Connor and Harvey* [2008], and P and R are the volumetric production and uptake (combination of processes consuming dissolved oxygen) rates of dissolved oxygen, respectively. Fitting the measured dissolved oxygen concentration profiles to equation (6) was performed using the PROFILE model, which fits the concentration profile to zones of net volumetric production using a statistical algorithm to minimize errors [*Berg et al.*, 1998].

[26] This patch-scale stream metabolism measurement technique is based on the conceptual model that dissolved oxygen production by photosynthesis occurs near the sediment-water interface and uptake varies with depth in the sediments. For the purposes of this analysis, the PROFILE model was set to include only two zones: a surface production zone and an uptake zone below (Figure S2 in the auxiliary material). The volumetric production and uptake rates were integrated over depth in the sediments to yield the net patch-scale production (NEP_{patch}) flux according to

$$NEP_{patch} = P\delta_p + R(\delta - \delta_p) \tag{7}$$

where δ_p is the depth of the production zone (inflection point in the measured concentration profile) and δ is the dissolved oxygen penetration depth (where $C = 0$).

4. Results

4.1. Storm-Induced Flow Pulses and Diel Dissolved Oxygen Concentrations

[27] April through October precipitation totals were 73.2 cm in 2005, 75.2 cm in 2006, 117.7 cm in 2007, and 93.5 cm in 2008. Discharges were largest in spring and early summer, followed by base flow conditions during the fall in 2005 and 2008, whereas flow peaks were found throughout spring to fall periods in 2006 and 2007 (Figure S1 in the auxiliary material). Correlations between daily precipitation totals and daily averaged discharges were not significant but depicted less runoff generation during periods where crop cover was present (15 June through 30 September each year; Figure S3 in auxiliary material). A positive trend between ΔDO with incoming solar radiation and a negative trend with daily precipitation were observed but with much scatter in the data (Figures 3a and 3b). The correlation between ΔDO and discharge was stronger, and was approximated by a power function but also suggests a threshold-type relationship (Figure 3c).

[28] Dissolved oxygen concentrations varied by as much as 8 mg/L in a day with mean concentrations on the order of 10 mg/L under steady to declining discharge conditions (Figure 4). Peaks in discharge coincided with periods when the diel dissolved oxygen concentration fluctuations were minimal. In Figure 4, the large flood that occurred in late June 2007 showed a steady trend of increasing fluctuations in diel dissolved oxygen concentrations during the postflood succession period. The multiple floods that occurred later in the summer and fall corresponded with several interruptions in the fluctuating diel dissolved oxygen concentration signal. The fluctuating diel dissolved oxygen concentration pattern was represented as ΔDO values as shown in Figure 5 for 2005 through 2008. During steady to declining flow conditions, ΔDO values were on the order of 4 to 8 mg/L. Peaks in discharge corresponded with a rapid decline in ΔDO values below 2 mg/L. The recovery period of the ΔDO values back to the 4 to 8 mg/L range varied in relation to the magnitude of the peak discharge, the number of discharge peaks, and the seasonal time frame that the discharge peaks occurred.

[29] Peaks in discharge, or flow pulses, vary in magnitude with respect to the amount of precipitation, as well as the prevailing flow conditions prior to the storm event. Flow pulses were identified as changes in daily averaged discharge of greater than 25% to account for seasonally varying flow conditions. Detected flow pulses are shown in Table 1, where the dates indicate the initial date of the flow pulse along with the resulting peak discharge (Q_p) and the percent change in discharge (ΔQ). The time period to reach Q_p ranged between 1 and 4 days with an average value of 2 days.

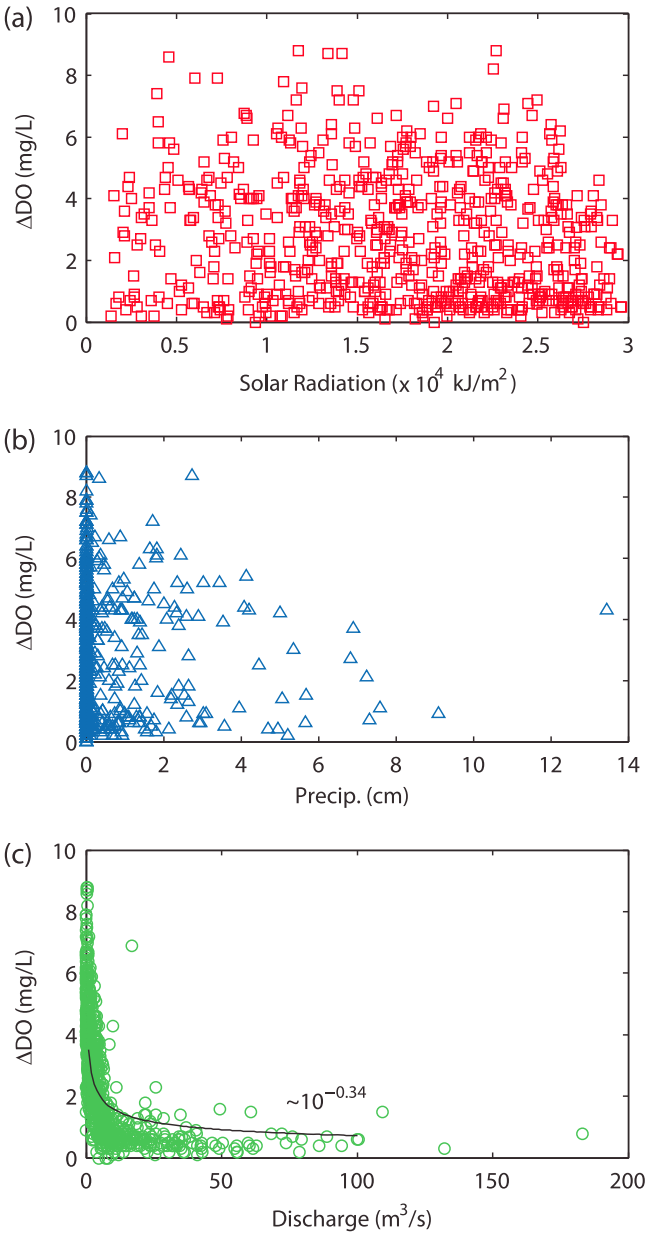

Figure 3. Correlations between ΔDO values and (a) solar radiation, (b) daily precipitation, and (c) daily averaged discharge.

Flow-induced disturbances to the ΔDO signal were detected as values that fell below a threshold value with recovery periods being identified as the time for ΔDO values to recover above the threshold value. This analysis was performed using threshold ΔDO values of 1.5 and 2 mg/L, which produced similar results with respect to disturbance date and some variability with respect to the recovery period. The ΔDO disturbance dates listed in Table 1 correspond to the 2 mg/L threshold. The recovery periods listed in Table 1 correspond to the range in recovery periods based on the 1.5 and 2 mg/L ΔDO thresholds, as well as data gaps existing in the ΔDO record.

[30] Flow pulses identified by this analysis ranged in Q_p from less than 1 to over 150 m^3/s with corresponding ΔQ values ranging from 25 to over 5000% (Table 1). Disturbances to ΔDO values typically occurred in response to flow pulses where ΔQ was greater than 100%, a notable exception being the disturbance that occurred on 22 September 2005 in response to a ΔQ of 36% (Table 1). Recovery periods for ΔDO ranged from 1 to more than 40 days, with approximately 70% of the detected disturbances having recovery periods on the order of 15 days or more and the remaining 30% on the order of 5 days or less. From late April to mid-June 2007, there were several flow pulses detected that coincided with the largest data gap in the ΔDO record, and other data gaps overlapped with the disturbance date and the end of the recovery period. In addition to issues pertaining to data gaps in the ΔDO record, disturbances and recovery periods of ΔDO are often not the result of a single flow pulse (Table 1 and Figure 5). For example, the ΔDO disturbance that occurred on 2 October 2007 was initiated by the flow pulse on the same day, but the recovery period was affected by flow pulses that occurred on 8 October 2007 and 14 October 2007 (Table 1).

4.2. Physical Habitat and Stream Metabolism During Steady Flow Conditions

[31] The main geomorphic features of the upstream portion of the study reach are the island bar and the riffle segments on either side of the island bar, while the downstream portion of the study reach is a straight channel with a fairly uniform cross section (Figure 1b). The sediment texture survey results indicate that the study reach was predominately gravel with sands and cobbles in patches. The top two sediment texture classes csG and sG represent 44% of the streambed (Table 2). The locations of the sediment texture classes and the coverages of green algae and FBOM are shown in Figures 6a–6c. The island bar was classified as sand (texture class, S) because the majority of the northern side of the bar was an eddy depositional area downstream of the riffle, and vegetated portions of the island bar on the southern side were not inundated during the flooding event

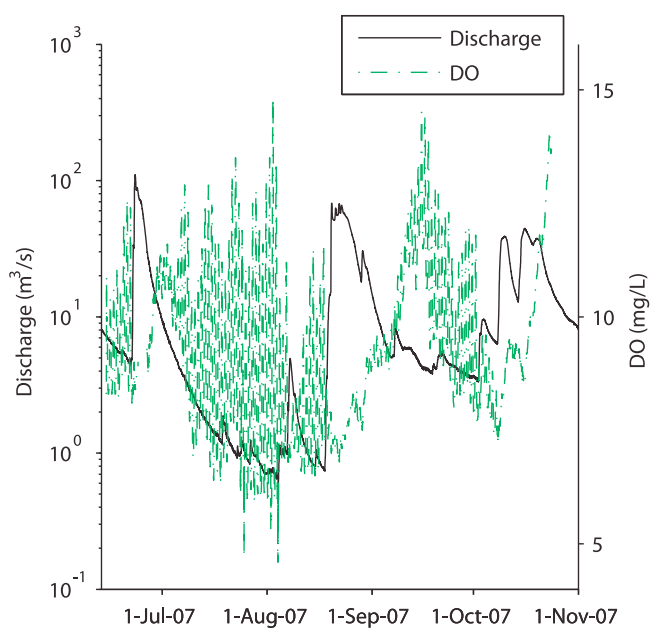

Figure 4. Discharge and dissolved oxygen concentrations measured on the South Fork Iowa River in 2007.

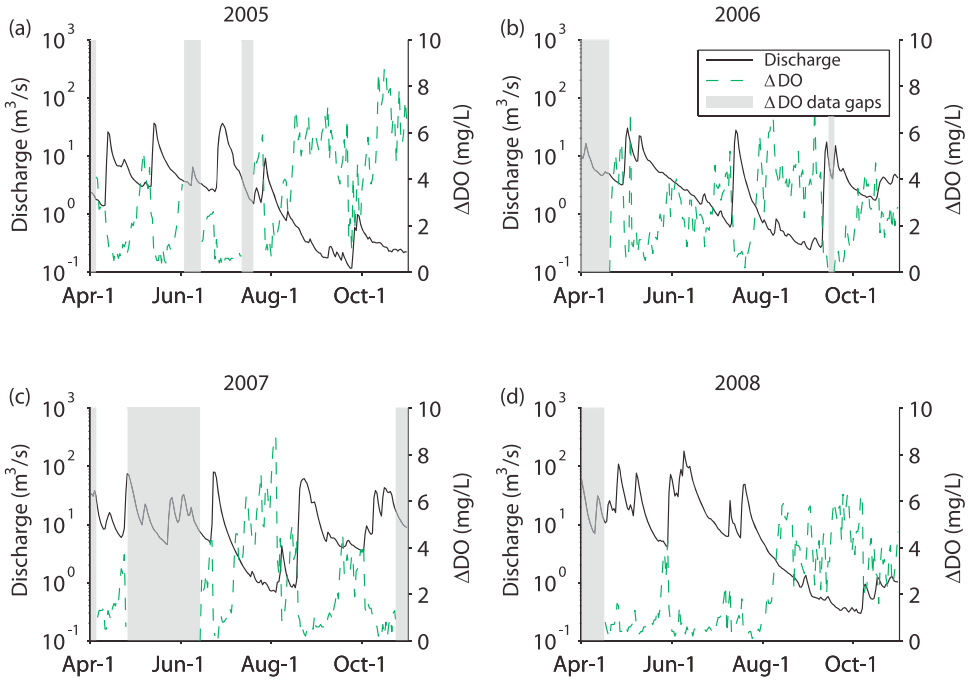

Figure 5. Discharge and ΔDO values (difference in daily minimum and maximum dissolved oxygen concentrations) measured on the South Fork Iowa River in (a) 2005, (b) 2006, (c) 2007, and (d) 2008.

of 2 October 2007 (Figure 2). Green algae was predominately associated with sediment texture classes containing gravels and cobbles while FBOM was most prevalent along the stream banks and finer particle sizes (Figures 6b and 6c and Table 2).

[32] Hydraulic modeling of the study reach for steady flow conditions of 1 October 2007 demonstrated high velocities and bed shear stresses associated with the riffle regions on each side of the island bar (Figures 6d and 6e). Effective diffusion values (hyporheic exchange potential) were greatest at the head of the riffle located on the north side of the island bar (Figure 6f). Water velocities were greatest over the csG, sG, and G sediment texture classes (Table 3), which primarily represent the sediment substratum of the thalweg portion of the channel (Figure 6a). Bed shear stress was largest and most variable over the sgC sediment texture class (Table 3), which is mostly associated with the riffle located on the south side of the island bar (Figure 6a). Hydraulic conductivity was greatest for gS and S sediment texture classes, but effective diffusion was greatest for gS and G sediment texture classes, indicating that hyporheic potential over S sediment texture patches was limited by hydraulic forcing (Table 3).

[33] Examining the combination of sediment texture patches, channel bathymetry, and hydraulics over the study reach suggests that there were specific regions that can be categorized as fixed, free, or forced patches (Figures 1b, 6a, 6d, and 6e). The riffle segments on either side of the island bar represent fixed patches located at topographic high points containing coarser sediments. The channel along the south side of the island bar contains more cobble sediments and a fairly armored bed near the riffle (sgC sediment texture class). In addition, high percentages of green algal coverage are associated with the southern riffle region (Figure 6b), which suggests this patch has remained relatively fixed in place over an extended period of time. The eddy depositional area along the north side of the island bar (depicted in Figures 1b and 2) represents a forced patch that has remained in place because of the topographic high point and vegetative cover of the upper portion of the island bar. The channel along the north side of the island bar and downstream of the riffle is primarily unconsolidated sands and gravels (sG sediment texture class) that represent a free patch where the sediments have characteristics similar to those described as bed load sheets [*Whiting et al.*, 1988].

[34] Patch-scale metabolism measurements consisting of dissolved oxygen profiles were performed at sampling stations 2–4, shown in Figure 1a. These measurements were taken during steady flow conditions (Q = 3.3 m^3/s) on 1 October 2007. Dissolved oxygen profiles show a wide range in concentrations at the sediment-water interface ranging between 8.5 and 11 mg/L with penetration depths (δ) ranging from 2 to 10 cm (Figure 7a). Measurements at station 2 consisted of two profiles, one within the submerged portion of the eddy bar (S sediment texture class) and the other within the shallow pool downstream of the northern riffle (sG sediment texture class). The eddy bar location had the largest dissolved oxygen production (P) and uptake (R) rates, as well as the highest percentage of FBOM coverage among measurement locations (Figure 7b). The shallow pool location consisted of loosely consolidated gravels and sands and had the largest δ of 10 cm. The resulting NEP_{patch} values at these locations were −1.8 g $O_2/m^2/d$ in the eddy bar (S) location and −16.4 g $O_2/m^2/d$ in the shallow pool (sG) location (Table 4, a negative NEP_{patch} indicates a net removal of dissolved oxygen from the river). Stations 3 and 4 were located in the downstream portion of the study reach with station 3 within the G sediment texture class and station 4 within the csG sediment texture class. Measured NEP_{patch} values were −2.8 g $O_2/m^2/d$ at station 3 and 2.3 g $O_2/m^2/d$ at station 4, which represents the only positive NEP_{patch} measured and

Table 1. Flow Pulses and Disturbances to The ΔDO Signal

Flow Pulse			ΔDO Disturbance	
Date	Q_p (m^3/s)	ΔQ (%)	Date	Recovery Period (days)
Average Precipitation Years				
2005				
			(ΔDO data gap 1–4 Apr)	
11 Apr	25.9	1728	12 Apr	15–17
12 May	36.5	1105	14 May	15–16
			(ΔDO data gap 2–14 Jun)	
8 Jun	6.4	107	15 Jun [a]	>10
25 Jun	32.1	1021	24 Jun	19–26[b]
			(ΔDO data gap 12–19 Jul)	
20 Jul	2.3	55		
25 Jul	9.1	476	28 Jul	9–10
11 Aug	1.1	45		
8 Sep	0.3	52		
17 Sep	0.2	36	22 Sep	3–4
24 Sep	1.0	729		
2006				
			(ΔDO data gap 1–20 Apr)	
3 Apr	16.4	47		
29 Apr	30.2	825	30 Apr	23–24
9 May	22.2	170		
21 Jun	2.1	36		
11 Jul	27.7	3899	12 Jul	13–15
9 Aug	0.8	75		
2 Sep	0.3	25		
10 Sep	17.3	5802	11 Sep	20–21[c]
			(ΔDO data gap 13–18 Sep)	
17 Sep	15.0	270		
17 Oct	3.6	80	19 Oct	5–7
27 Oct	4.53	29		
Above Average Precipitation Years				
2007				
			(ΔDO data gap 1–5 Apr)	
1 Apr	36.8	505	6 Apr[a]	15–19
11 Apr	11.2	32	(ΔDO data gap 24 Apr to 14 Jun)	
23 Apr	75.1	1035	(ΔDO data gap 24 Apr to 14 Jun)	
6 May	22.5	129	(ΔDO data gap 24 Apr to 14 Jun)	
23 May	26.5	482	(ΔDO data gap 24 Apr to 14 Jun)	
31 May	31.0	158	(ΔDO data gap 24 Apr to 14 Jun)	
7 Jun	19.7	36	(ΔDO data gap 24 Apr to 14 Jun)	
21 Jun	79.6	1570	23 Jun	13–14
4 Aug	4.3	529	8 Aug	3–4
17 Aug	55.0	6671	19 Aug	25–26
7 Sep	7.4	44		
2 Oct	9.5	177	2 Oct	>22[d]
8 Oct	38.4	443		
14 Oct	43.0	208	(ΔDO data gap 24–31 Oct)	
2008				
			(ΔDO data gap 1–16 Apr)	
10 Apr	31.1	345	(ΔDO data gap 1–16 Apr)	
18 Apr	21.7	91	17 Apr[a]	>38
24 Apr	109.5	582		
6 May	76.3	440		
29 May	72.3	1654	30 May	37–38
5 Jun	183.1	510		
7 Jul	25.7	308	Jul-8	24–26
17 Jul	47.8	710		
28 Aug	1.2	27		
7 Oct	0.8	135	8 Oct	1–2
15 Oct	1.2	120	18 Oct	1–2

[a]Disturbance date within data gap.
[b]Recovery date within data gap.
[c]Recovery period spans data gap.
[d]Recovery period extends into data gap.

coincides with the largest percent algal coverage of the sampling locations (Figure 7b).

[35] Reach-scale metabolism measurements during steady flow conditions of 1 October 2007 show the typical pattern of a negative NEP during the night and positive during the day time hours (Figure 8b). During the day, GPP values range from 0 to 45 g $O_2/m^2/d$ while NEP ranged from 0 to 30 g $O_2/m^2/d$. CR values were typically on the order of −20 g $O_2/m^2/d$ with daytime values estimated by linear interpolation between dawn and dusk. Daily averaged values of GPP, CR, and NEP were 11.0, −16.6, and −5.6 g $O_2/m^2/d$, respectively. The daily range in GPP falls within the range of patch-scale measurements of the production flux ($P\delta_p$), except the measurements at station 2 within the S sediment texture class (Table 4). Patch-scale measurements of uptake flux ($R(\delta - \delta_p)$) were all greater than the daily range in CR values, while the net production values at the patch scale (NEP_{patch}) at all measurement locations were of similar magnitude to the reach-averaged NEP value (Table 4).

4.3. Storm Disturbance Effects on Stream Metabolism

[36] The storm event on 2 October 2007 delivered over 5 cm of rainfall over a 7 h period that resulted in a change in discharge from 3.1 to 6.9 m^3/s (Figure 8a). Reach-averaged metabolism rates of GPP, CR, and NEP were all shifted toward net respiration during the storm event in comparison to the values of the previous day under steady flow conditions (Figure 8b). GPP was reduced from a daily maximum of 45 g $O_2/m^2/d$ on 1 October 2007 to a daily maximum of 16 g $O_2/m^2/d$ during the storm event on 2 October 2007. NEP and CR values were both negative throughout the day on 2 October 2007.

[37] The effect of the storm-induced flow disturbance on sediment bed mobility was assessed by comparing the ratio of τ^*/τ_c^* where values greater than one would indicate incipient motion of the sediment bed. Figures 9 and 10 show maps of τ^*/τ_c^* computed over the study reach from prestorm to poststorm conditions for τ_c^* values equal to 0.0495 and 0.03, respectively (see the auxiliary material for time-lapse Animation S1 of bed shear stress and stream metabolism values during the storm event). Prior to the storm, τ^*/τ_c^* values indicated isolated regions where the incipient motion threshold was surpassed for both τ_c^* values; these locations were primarily within gS sediment texture classes (Figures 6a, 9a, and 10). During the storm, as discharge increased the island bar was inundated and showed increasing τ^*/τ_c^* values (Figures 2, 9, and 10). Increasing τ^*/τ_c^* values during the storm event were also observed along the north bank of the upper portion of the reach, along the head of the island bar, and along the north bank in the downstream portion of the study reach (Figures 9b–9f and 10b–10f). Large portions of the study reach did not experience τ^*/τ_c^* values above the threshold for incipient motion for both the high and low τ_c^* values considered, and these immobile regions primarily followed the southern side of the island bar and downstream reach, which were associated with sediment texture classes containing cobbles (Figures 6a, 9b–9f, and 10b–10f). The primary difference in the maps of τ^*/τ_c^* between the high and low τ_c^* values were associated with the inundation of the island bar where incipient motion thresholds were surpassed earlier

Table 2. Sediment Substratum Characteristics According to Sediment Texture Classes

Sediment Texture Class	Streambed Coverage (m^2)	Streambed Coverage (%)	d_{90} (cm)	d_{50} (cm)	FBOM (% Coverage)	Green Algae (% Coverage)
Cobbley sandy gravel, csG	1057	22.6	6.0	2.0–6.4	0–50	0–50
Sandy gravel, sG	1014	21.7	2.5	0.6–2.0	0–100	0–20
Gravel, G	568	12.2	6.0	0.6–2.0	0–50	0–16
Sandy gravelly cobble, sgC	566	12.1	12.0	6.4–12.8	0–38	0–38
Sand, S	446[a]	9.6	2.0	0.006–0.2	0–25	0
Gravelly sand, gS	368	7.9	6.0	0.006–0.2	0–25	0–30
Silty sand, zS	342[b]	7.3	3.0	0.006–0.2	0–63	0–25
Silty cobble, zC	300	6.4	22.0	6.4–12.8	0–11	0–25
Silty gravel, zG	9	0.2	22.0	6.4–12.8	0–11	0–29

[a]75% of sand texture class (S) is located adjacent to island bar.
[b]40% of silty sand texture class (zS) is located along stream banks.

in the flood event with the lower τ_c^* value (Figures 9d–9f and 10d–10f).

[38] Median values of τ^*/τ_c^* associated with each sediment texture class throughout the storm event are shown in Figures 11a and 11b considering both the high and low values of τ_c^*. The storm event occurred from 10:30 AM to 5:30 PM, and prior to the storm median τ^*/τ_c^* were above the incipient motion threshold for the gS texture class only. According to Figure 6a, the gS texture classes are primarily located in isolated regions along the northern bank and represent approximately 8% of the total study reach area (Table 2). As discharge increased during the storm event, the median τ^*/τ_c^* values went above the incipient motion threshold for both the S and zS sediment texture classes. The low τ_c^* value suggested that incipient motion for the S and zS sediment texture classes occurred at 12 PM when the discharge had increased from 3.1 to 3.2 m^3/s (Figure 11b), whereas the high τ_c^* value suggested these patches were mobilized at 4 PM when discharge had increased to 4.0 m^3/s (Figure 11a). By 7:30 PM, the discharge reached 6.5 m^3/s and median τ^*/τ_c^* values exceeded incipient motion threshold for the zG sediment texture class for both the high and low τ_c^* values. Over the course of the storm event, median τ^*/τ_c^* values were steady and below incipient motion threshold conditions for csG, sG, G, sgC, and zC sediment texture classes for both the high and low τ_c^* values (Figure 11).

5. Discussion

[39] The South Fork Iowa River has little riparian shading, high nutrient concentrations, and abundant periphyton communities that result in high photosynthesis rates during the day and high respiration rates during the night, which is typical for agricultural rivers [*Young and Huryn*, 1999; *Houser et al.*, 2005; *Morgan et al.*, 2006]. The high photosynthesis and respiration rates in agricultural rivers result in large diel fluctuations in DO concentrations. These large fluctuations in diel DO concentrations can be quantified as ΔDO values, which have been shown to correlate with stream metabolism metrics of NEP, GPP, and CR for streams under steady flow conditions [*Mulholland et al.*, 2005]. The main shortfall of using ΔDO as a surrogate measure of stream metabolism is that is does not incorporate the effects of discharge on K_2, and the Q - K_2 relationship is difficult to determine and often site specific [e.g., *Izagirre et al.*, 2008]. The goal of this study was to examine flow disturbance impacts on stream metabolism, and the use of ΔDO provided a simple measure that allowed for the assessment of disturbance and recovery times of stream metabolism. In the South Fork Iowa River, peaks in discharge (flow pulses) were correlated to storm-induced precipitation events (Figure S1 in the auxiliary material), as well as to disruptions of the ΔDO signal (Figure 5 and Table 1). These results, and those of other studies, suggest that stream metabolism is highly sensitive to flow disturbances, as well as land use factors affecting rainfall-runoff processes such as extensive drainage in agricultural watersheds [*Uehlinger and Naegeli*, 1998; *Uehlinger*, 2000; *Houser et al.*, 2005; *Mulholland et al.*, 2005; *Uehlinger*, 2006].

[40] The examination of the 4 year record of discharge and ΔDO values at the South Fork Iowa River suggested that changes in daily averaged discharge of greater that 100% resulted in a disruption to the ΔDO signal (Table 1). The threshold condition defining a disruption to the ΔDO signal corresponded to flows typically greater than 25 m^3/s (Figure 3), but there were several recorded disturbances to the ΔDO signal at lower discharges (Table 1). Therefore, there was no discharge magnitude that represented a threshold condition for stream metabolism. Recovery periods of the ΔDO signal fell into two categories of less than 5 days or greater than 15 days. The observed pattern of distinct short- and long-recovery periods of the stream metabolism signal suggests that there are threshold conditions governing the relationship between flow disturbance and stream metabolism, but there were no specific discharge values that determined the recovery period of the stream metabolism signal (Figure 5 and Table 1). In addition, there were several instances where multiple flow pulses occurred affecting the recovery period of the ΔDO signal (Figure 5).

[41] Previous studies have used specific discharge values for describing flow thresholds relating to stream metabolism [*Uehlinger and Naegeli*, 1998; *Uehlinger*, 2000, 2006; *Atkinson et al.*, 2008]. This approach can be problematic, given that the primary mechanism for flow disturbance impacts on stream metabolism is via bed shear stress effects on periphyton and sediment transport [*Biggs et al.*, 1999; *Cronin et al.*, 2007], which is primarily controlled by turbulence and sediment interactions rather than the magnitude

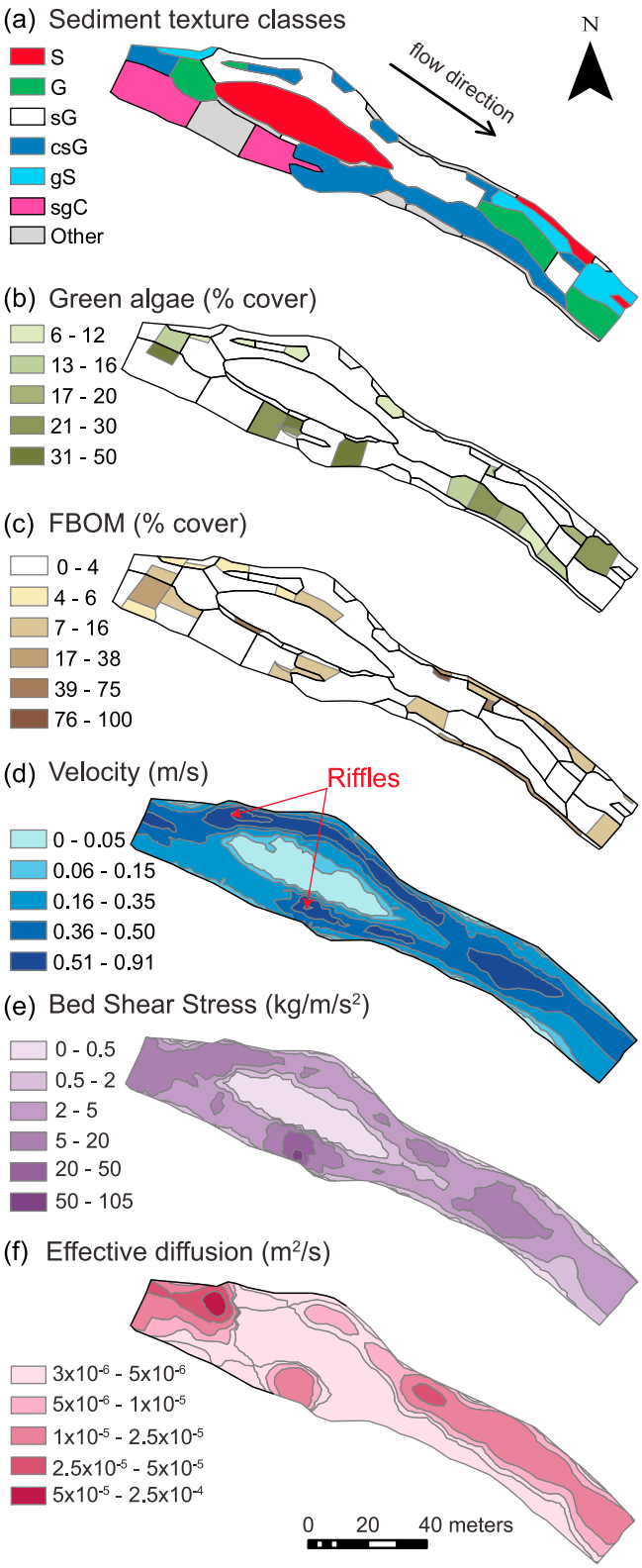

Figure 6. Physical habitat and hydraulic variable maps of the South Fork Iowa River study reach for steady flow conditions of 1 October 2007: (a) sediment texture class, (b) green algae coverage, (c) fine benthic organic material (FBOM) coverage, (d) depth-averaged velocities, (e) bed shear stress, and (f) estimates of effective diffusion (hyporheic exchange potential).

of the flow. Understanding how flow disturbances affect bed shear stresses requires knowledge of the physical habitat conditions described by the hydraulics, geomorphology, and sediment conditions in a river. In addition, patch-scale variability in physical habitat conditions greatly affect algal abundance and community structure [*Munn et al.*, 2010; *Ogdahl et al.*, 2010], so physical processes governing bed mobility occurring at the patch scale affect the relationship between flow disturbance and stream metabolism. For the South Fork Iowa River, there were two distinct groupings of stream metabolism recovery periods and a variety of discharge-related conditions that affected stream metabolism. The mechanisms governing these patterns were hypothesized to relate to subreach variability in sediment habitats for stream metabolism and how these habitats responded individually to flow disturbances. Specifically, flow disturbances were considered to mobilize either a portion or the majority of the streambed resulting in corresponding short- and long-recovery periods of stream metabolism.

[42] The physical habitat of the study reach was assessed using visual mapping techniques to identify sediment texture patches according to the method of *Buffington and Montgomery* [1999], and larger-scale free, forced, and fixed regions [e.g., *Nelson et al.*, 2009]. The upper half of the study reach included an island bar that created two channels where the northern channel contained sand and gravel sediments (sG and csG sediment textures classes), and the southern channel contained cobble and gravel sediments (sgC and csG sediment texture classes); the lower half of the study reach was mostly gravel and sand (Figure 6a). The coarser cobbles in the southern channel of the upper reach (which extended along the southern portion of the lower reach as well) constituted a fixed sediment texture region of armored sediments, which have the ability to persist even during floods [*Wilcock and DeTemple*, 2005]. The cobble sediments of the southern channel also contained the greatest densities of green algae in the study reach (Figure 6b), suggesting that these sediment texture patches were relatively stable during the several flood flows that occurred previously in 2007 (Figure 5c). The thalweg of the northern channel in the upper reach and most of lower reach (with exception to cobbles along the southern bank) represented a free sediment texture region where the sand and gravel sediments showed indications of sediment transport from previous floods including the presence of bed load sheets [*Whiting et al.*, 1988]. Portions of the island bar of gently sloped sands along the northern channel represented a forced sediment texture patch, most of which only becomes active once water levels rise (Figure 2).

[43] Patch-scale stream metabolism rates varied amongst sediment texture classes, but the largest volumetric production (P) and uptake (R) rates were recorded in the S sediment texture class at station 2 (Figure 7). This location is within the submerged portion of the forced sediment texture region of S sediment texture class associated with the island bar (Figures 1b, 2, and 6a). The only patch-scale metabolism measurement that had a net production flux (positive NEP_{patch} value) was at station 4 in the csG texture class (portion of the fixed cobble sediment texture region, Figure 7). The production flux ($P\delta_p$), uptake flux ($R\delta - R\delta_p$), and NEP_{patch} values for the South Fork Iowa River (Table 4) were larger

Table 3. Modeled Hydraulic Variables and Measured Hydraulic Conductivity by Sediment Texture Classes During Steady Flow Conditions of 1 October 2007[a]

Sediment Texture	Depth h (cm)	Velocity u (cm/s)	Bed Shear Stress τ_b (N/m^2)	Effective Diffusion D_e (m^2/s)	Hydraulic Conductivity K_c (cm/s)
csG	35.3 (28.6–46.9)	43.3 (33.6–50.3)	4.35 (2.81–5.73)	2.68×10^{-6} (1.33×10^{-6} to 6.56×10^{-6})	0.004
sG	29.8 (19.9–44.0)	40.0 (26.5–54.0)	3.27 (1.91 – 4.74)	5.17×10^{-6} (2.42×10^{-6} to 9.54×10^{-6})	0.096
G	35.2 (27.9–41.3)	41.9 (26.0–52.8)	4.70 (2.37–6.91)	1.21×10^{-5} (7.75×10^{-6} to 2.04×10^{-5})	0.065
sgC	43.5 (31.4–52.5)	32.7 (25.2–42.8)	7.72 (4.03–12.62)	8.11×10^{-6} (4.42×10^{-6} to 1.47×10^{-5})	0.004
S	5.5 (3.8–14.0)	7.9 (1.6–21.6)	0.20 (0.01–1.36)	2.80×10^{-7} (8.52×10^{-9} to 2.82×10^{-6})	0.178
gS	49.7 (28.8–60.0)	38.4 (32.8–43.3)	3.49 (2.79–4.10)	2.01×10^{-5} (1.52×10^{-5} to 2.39×10^{-5})	0.180
zS	21.2 (13.9–33.2)	15.6 (6.0–25.8)	0.85 (0.32–2.09)	6.33×10^{-7} (1.57×10^{-7} to 2.68×10^{-6})	0.000
zC	56.8 (43.9–69.8)	21.6 (15.8–27.2)	3.20 (2.27–3.94)	2.65×10^{-6} (1.53×10^{-6} to 3.60×10^{-6})	0.001
zG	18.8 (13.9–21.2)	0.8 (0.1–2.6)	0.03 (0.00–1.19)	1.49×10^{-8} (1.04×10^{-9} to 1.02×10^{-6})	0.001

[a]Median values shown with 25th and 75th percentile values shown in parentheses.

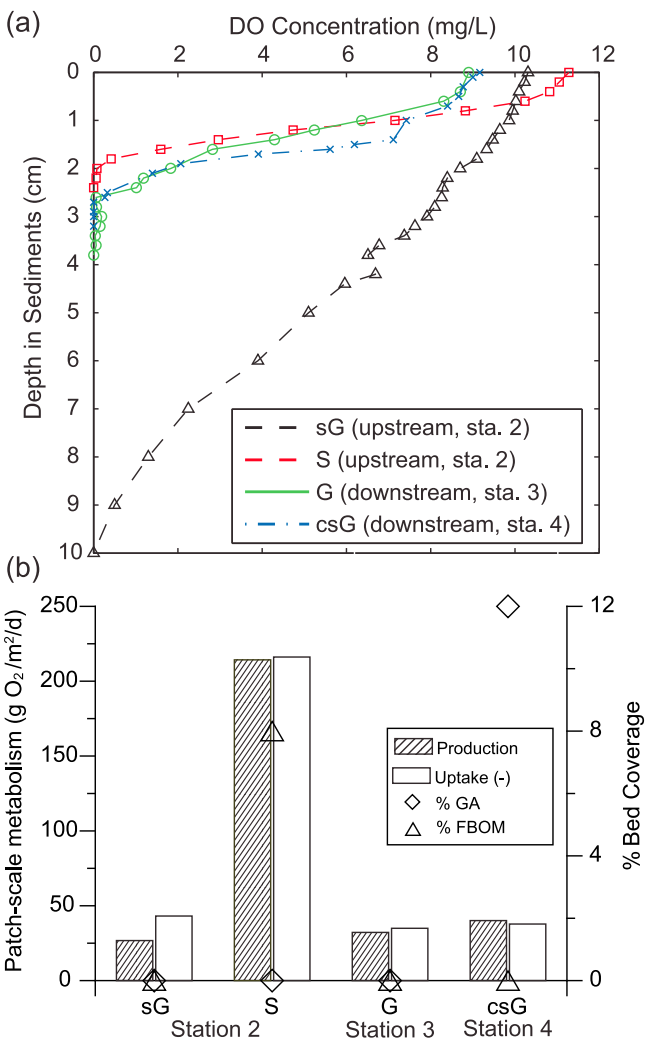

Figure 7. Patch-scale metabolism measurements derived from (a) dissolved oxygen profiles and (b) calculated production and uptake fluxes according to equations (6) and (7).

than values previously reported in other studies examining patch-scale variability in stream metabolism rates. *Cardinale et al.* [2002] used chamber mesocosms in a forested stream and recorded production fluxes ranging from 0 to 4.8 g $O_2/m^2/d$ and uptake fluxes ranging from 0 to −1 g $O_2/m^2/d$. *Wilson and Dodds* [2009] used microsensor-based measurements of NEP_{patch} (similar to this study) in a prairie stream with values ranging between −0.1 and +0.3 g $O_2/m^2/d$. Patch-scale stream metabolism rates are expected to vary between forested, prairie, and agricultural streams; however, differences arising between mesocosm chambers and microsensor profile-based measurements of stream metabolism are not fully understood. The main difference between the NEP_{patch} results of this study and those of *Wilson and Dodds* [2009] was our use of the effective diffusion coefficient (D_e) over the molecular diffusion coefficient in equation (6), which has been shown to significantly affect flux calculations from concentration profiles [*O'Connor and Harvey*, 2008].

[44] The prestorm, daily averaged value of NEP measured at the South Fork Iowa River was bounded by the patch-scale measurements of NEP_{patch} (Table 4). In addition, the measured NEP value was of similar magnitude to values reported across a variety of biomes [*Mulholland et al.*, 2001], and in agricultural watersheds [*Frankforter et al.*, 2010]; however, daily averaged GPP and CR values were similar to the largest values recorded in these studies. During steady flow conditions before the storm GPP values ranged between 0 and 45 g $O_2/m^2/d$, but the storm event on 2 October 2007 reduced the range in daytime GPP values to 0 and 16 g $O_2/m^2/d$. Conversely, CR values during the nighttime increased from −20 g $O_2/m^2/d$ before the storm to −35 g $O_2/m^2/d$ after the storm (Figure 8). The shift from a moderate- to a high-net respiration system in response to the flow disturbance was suspected to be the result of decreasing photosynthesis from increased turbidity and the loss of algal assemblages to drift, as well as an increase in heterotropic uptake caused by the increased delivery of organic material to the water column and sediment surface.

[45] The storm event on 2 October 2007 more than doubled the discharge during the daytime period, which resulted

Table 4. Patch- and Reach-Scale Metabolism Measurements During Steady Flow Conditions on 1 October 2007

	Production ($g\ O_2/m^2/d$)	Uptake ($g\ O_2/m^2/d$)	Net Production ($g\ O_2/m^2/d$)
Patch-scale	$P\delta_p$	$R(\delta - \delta_p)$	NEP_{patch}
Station 2 (S)	214.3	−216.2	−1.8
Station 2 (sG)	26.7	−43.13	−16.4
Station 3 (G)	32.2	−35.0	−2.8
Station 4 (csG)	40.1	−37.8	2.3
Reach-Scale	GPP	CR	NEP
Daily averaged	11.0	−16.6	−5.6

in portions of the island bar and stream banks becoming inundated, as well as an increase in bed shear stress to portions of the reach (Figures 9 and 10). The corresponding effects of the flow disturbance on stream metabolism is shown in Animation S1 in the auxiliary material. Uncertainty in our estimates of bed shear stress arising from the visual based estimates of particle sizes (d_{50} and d_{90}) can influence the results of a Shields stress criteria analysis of bed mobilization. In this study, the uncertainty in quantifying bed mobilization was accounted for by considering a high and low τ_c^* threshold value to bound the analysis. Results were consistent for both the high and low τ_c^* threshold values with the main difference being in the timing and the degree of mobilization of specific sediment texture patches. In additions, both analyses for the high and low τ_c^* values were consistent in predicting nonmobilization conditions for the remaining sediment texture patches (Figures 9, 10, and 11).

[46] The estimated Shields stress criteria (τ^*/τ_c^*, for both the high and low τ_c^* threshold values) suggested that only the gS, S, zS, and zG sediment texture classes were mobilized during the flow disturbance (Figures 11a and 11b), which together only represent 25% of the streambed area (Table 2). These sediment texture patches were primarily located adjacent to the island bar and along the stream banks, composed fine sediment particles, and coincided with large quantities of FBOM (Figure 6). The low τ_c^* threshold value suggested that the zS sediment texture was immediately affected by the onset of the storm event, which corresponds with timing of the initial alteration to the NEP signal (Figure 8b). The partial mobilization of finer sediments is consistent with the results of *Vericat et al.* [2008], which described a bed shear stress threshold below which sediment transport is dominated by fine sediment patches, and above which sediment transport is more uniform over a reach. In addition, fine particles mobilized during high flows typically have higher nutrient concentrations associated with them, making them more biologically active [*Harvey et al.*, 2011].

[47] The results of the 2 October 2007 storm event analyses depict a partial bed mobilization of sediment patches containing fine sediments, which suggests that the primary mechanism responsible for the disruption of stream metabolism was through increased turbidity rather than reach-scale bed mobilization. Fine sediment transport and increased turbidity limited photosynthesis by reducing light penetration, and stimulated respiration through the mobilization of fine, biologically active sediments. This effect of turbidity on stream metabolism has been shown for streams under steady flow conditions in watersheds where physical characteristics produce various turbidity levels [*Izagirre et al.*, 2008]. Because only a small portion of the total streambed (which includes algal and microbial communities) was disturbed, the storm-induced turbidity effect on stream metabolism would be suspected to have a short recovery time observable in the ΔDO signal. Unfortunately, this hypothesis could not be tested as two even larger floods occurred immediately following the 2 October 2007 flow disturbance (Table 1 and Figure 5c).

6. Summary

[48] This study used the analysis of discharge and ΔDO data to identify threshold behavior of stream metabolism response to flow disturbances. No specific discharge criteria could be identified that determined the observed grouping of short- or long-recovery periods of the stream metabolism signal. Physical habitat characterization and hydraulic modeling of storm event in the fall of 2007 showed that only

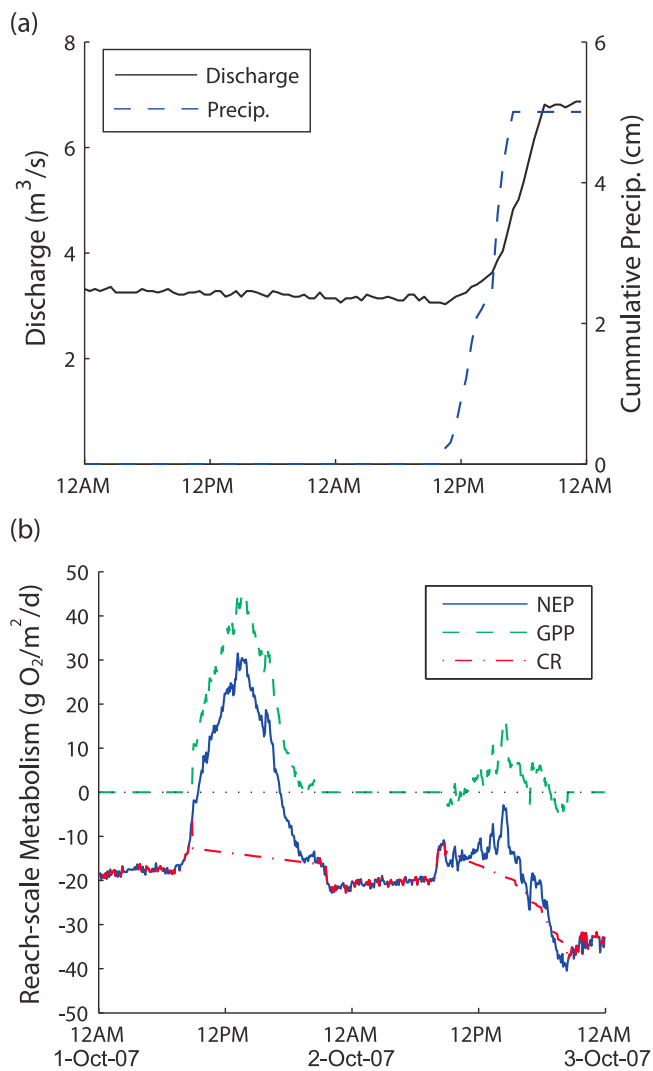

Figure 8. Reach-scale metabolism measurements of NEP, GPP, and CR under steady flow conditions of 1 October 2007 and the storm event on 2 October 2007: (a) discharge and cumulative precipitation and (b) reach-scale metabolism values for NEP, GPP, and CR.

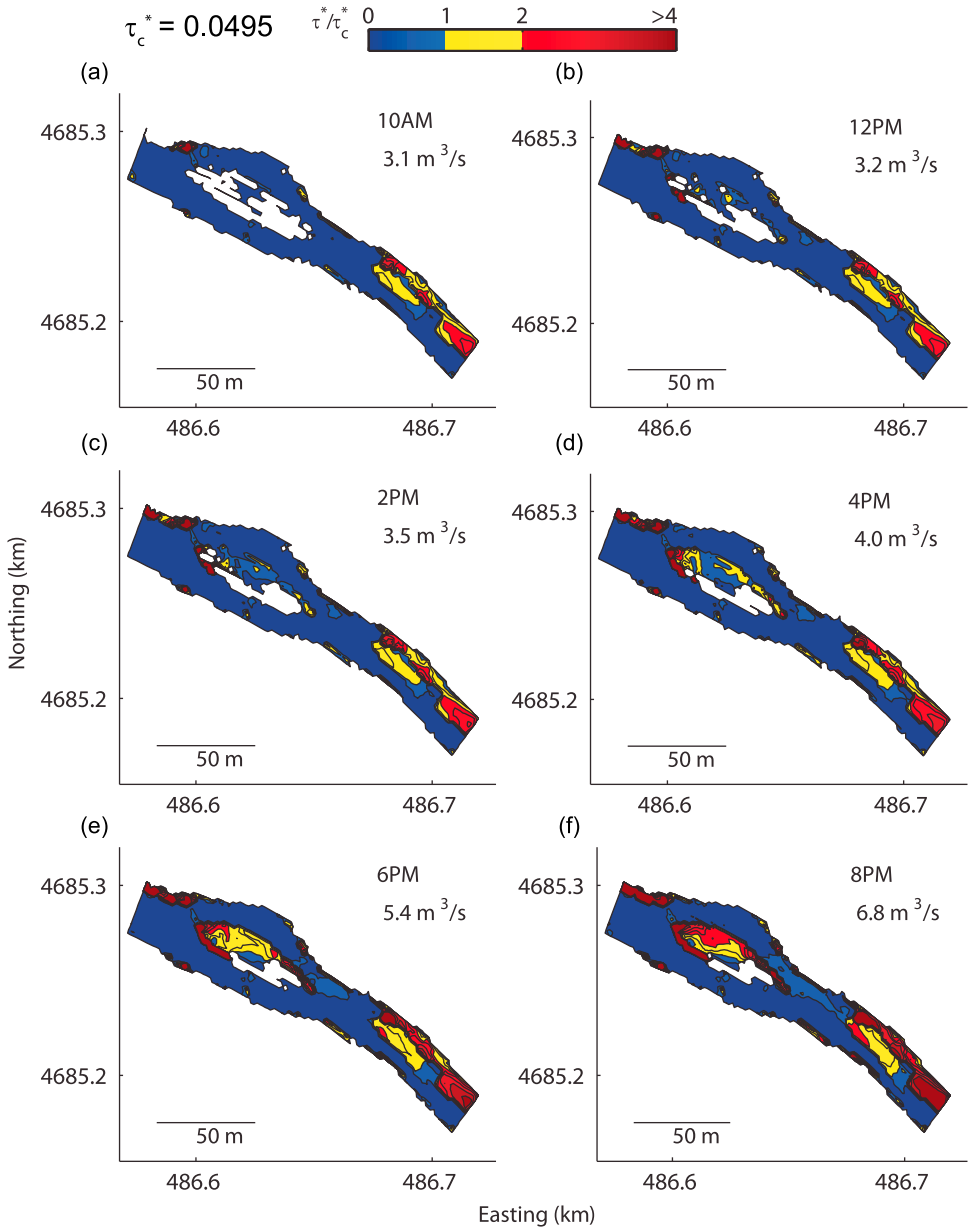

Figure 9. Maps of τ^*/τ^*_c values ($\tau^*_c = 0.0495$, high mobilization threshold) over the study reach during the storm event on 2 October 2007 at (a) 10 A.M., (b) 12 P.M., (c) 2 P.M., (d) 4 P.M., (e) 6 P.M., and (f) 8 P.M.

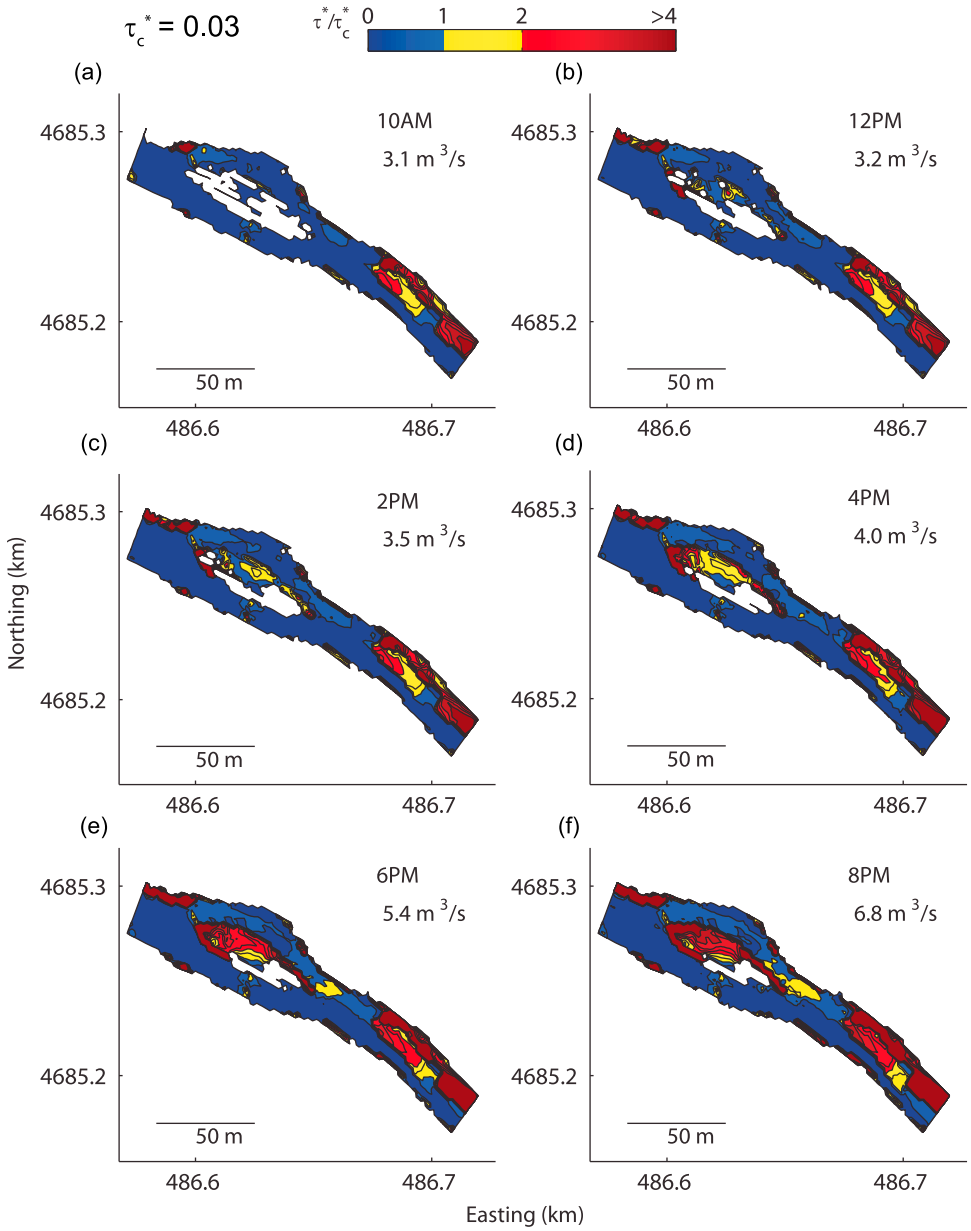

Figure 10. Maps of τ^*/τ^*_c values ($\tau^*_c = 0.03$, low mobilization threshold) over the study reach during the storm event on 2 October 2007 at (a) 10 A.M., (b) 12 P.M., (c) 2 P.M., (d) 4 P.M., (e) 6 P.M., and (f) 8 P.M.

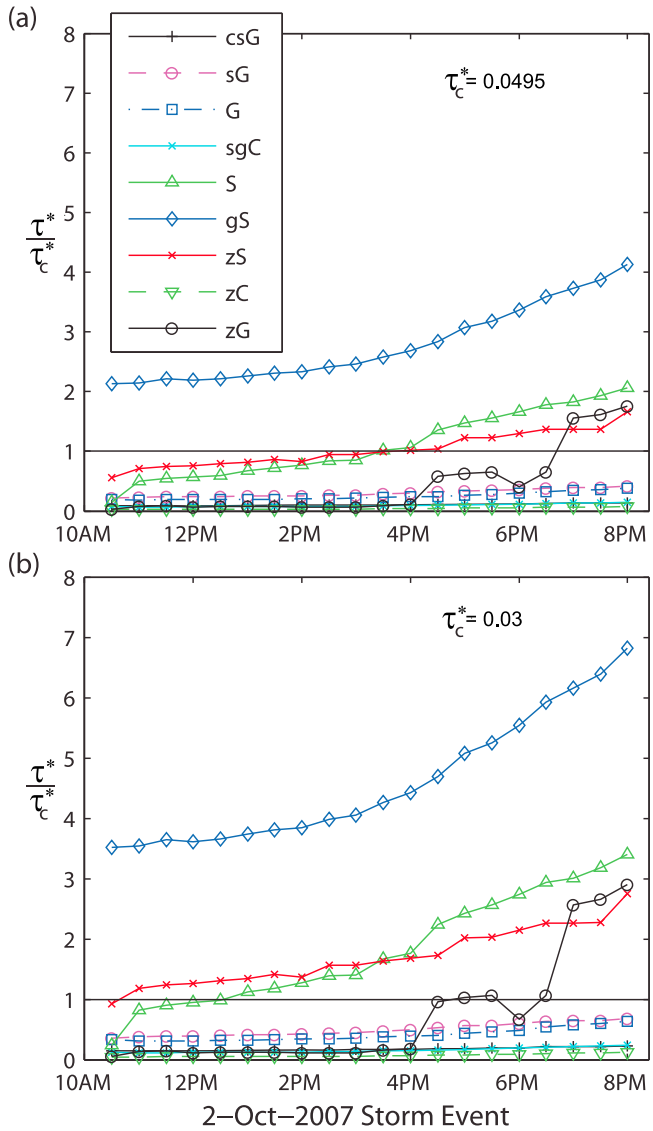

Figure 11. Median values of τ^*/τ^*_c according to sediment texture classes for the storm event on 2 October 2007 considering (a) the high mobilization threshold (τ^*_c = 0.0495) and (b) the low mobilization threshold (τ^*_c = 0.03).

25% of the streambed was mobilized. Of the streambed that was mobilized, most was associated with a forced sediment texture grouping of sand sediments along the island bar where patch-scale metabolism rates were largest. This evidence suggested that stream metabolism was primarily affected by increased turbidity and potentially some periphyton drift, rather than full bed mobilization, in response to the flow disturbance. This type of flow disturbance was hypothesized to be associated with the short-recovery period (less than 5 days) of stream metabolism, but the effect of multiple flow pulses acting on a single recovery period of stream metabolism could not be fully realized in this study. The results of this study support previous findings suggesting bed mobility is a primary factor affecting stream metabolism. In addition, this study extends this conclusion to the subreach scale, indicating threshold behavior in stream metabolism is the result of varying responses of sediment textural patches to partial or full bed mobilization by flow disturbances.

Notation

C dissolved oxygen concentration [M/L^3].
C_d drag coefficient.
CR community respiration [M/L^2/T].
D_e effective diffusion [L^2/T].
d_{50} median particle size [L].
d_{90} particle size for which 90% is finer [L].
GPP gross primary productivity [M/L^2/T].
g acceleration due to gravity [L/T^2].
H reach-averaged stream depth [L].
h stream depth [L].
K_2 reaeration coefficient [T^{-1}].
NEP net ecosystem production [M/L^2/T].
$\mathrm{NEP_{patch}}$ net patch-scale production [M/L^2/T].
P patch-scale production [M/L^3/T].
Q discharge [L^3/T].
Q_p peak discharge of flow pulse [L^3/T].
R patch-scale uptake [M/L^3/T].
R_p submerged particle specific gravity [M/L^3].
S reach-averaged slope.
T reach-averaged travel time [T].
t time [T].
U reach averaged velocity [L/T].
u streamwise velocity [L/T].
v transverse velocity [L/T].
y depth in sediments [L].
z_o roughness length [L].
ΔDO daily change in dissolved oxygen concentration [M/L^3].
δ DO penetration depth [L].
δ_p DO production zone depth [L].
κ von Kármán constant.
ρ water density [M/L^3].
τ_b bed shear stress [M/L/T^2].
τ^* Shields stress.
τ_c^* critical Shields stress.

[49] **Acknowledgments.** This study was performed while B. L. O'Connor held a National Research Council (NRC) Research Associateship Award at the U.S. Geological Survey (USGS) in Reston, Virginia. L. E. McPhillips was a research associate at the USGS when the study was performed. Funding for the study was provided by the National Water Quality Assessment (NAWQA) and National Research programs of the USGS, and NSF awards EAR0810140 and EAR 0814990 to USGS (J.W.H.). Field and logistical assistance was provided by Dan Nowacki, Leanna Westfall, Steve Kalkhoff, Dan Christiansen, and Mark Munn. Earlier versions of this manuscript were improved thanks to comments by Steve Kalkhoff and three anonymous reviewers. Any use of trade, firm, or product names is for descriptive purposes only and does not imply endorsement by the U.S. Government.

References

Arnon, S., A. I. Packman, C. G. Peterson, and K. A. Gray (2007), Effects of overlying velocity on periphyton structure and denitrification, *J. Geophys. Res.*, *112*, G01002, doi:10.1029/2006JG000235.

Atkinson, B. L., M. R. Grace, B. T. Hart, and K. E. N. Vanderkruk (2008), Sediment instability affects the rate and location of primary production and respiration in a sand-bed stream, *J. N. Am. Benthol. Soc.*, *27*(3), 581–592.

Bales, J. D., and M. R. Nardi (2007), Automated routines for calculating whole-stream metabolism: Theoretical background and user's guide, *Tech. Methods 4-C2*, 33 pp., U.S. Geol. Surv., Reston, Va.

Becher, K. D., S. J. Kalkhoff, D. J. Schnoebelen, K. K. Barnes, and V. E. Miller (2001), Water-quality assessment of the eastern Iowa

basins: Nitrogen, phosphorus, suspended sediment, and organic carbon in surface water, 1996–98, *U.S. Geol. Surv. Water Resour. Invest. Rep.*, *01-4175*.

Berg, P., N. Risgaard-Petersen, and S. Rysgaard (1998), Interpretation of measured concentration profiles in sediment pore water, *Limnol. Oceanogr.*, *43*, 1500–1510.

Biggs, B. J. F., R. A. Smith, and M. J. Duncan (1999), Velocity and sediment disturbance of periphyton in headwater streams: Biomass and metabolism, *J. N. Am. Benthol. Soc.*, *18*(2), 222–241.

Brunke, M., and T. Gonser (1997), The ecological significance of exchange processes between rivers and groundwater, *Freshwater Biol.*, *37*, 1–33.

Buchmiller, R. C., and D. A. Eash (2010), Floods of May and June 2008 in Iowa, *U.S. Geol. Surv. Open File Rep.*, *2010-1096*.

Buffington, J. M., and D. R. Montgomery (1997), A systematic analysis of eight decades of incipient motion studies, with special reference to gravel-bedded rivers, *Water Resour. Res.*, *33*(8), 1993–2029.

Buffington, J. M., and D. R. Montgomery (1999), A procedure for classifying textural facies in gravel-bed rivers, *Water Resour. Res.*, *35*(6), 1903–1914.

Bunte, K., and S. R. Abt (2001), Sampling surface and subsurface particle-size distributions in Wadable gravel- and cobble-bed streams for analyses in sediment transport, hydraulics, and streambed monitoring, *Gen. Tech. Rep. RMRS-GTR-74*, U.S. Dep. of Agric., Washington, D. C.

Cardinale, B. J., M. A. Palmer, C. M. Swan, S. Brooks, and N. LeRoy Poff (2002), The influence of substrate heterogeneity on biofilm metabolism in a stream ecosystem, *Ecology*, *83*(2), 412–422.

Cronin, G., J. H. McCutchan Jr., J. Pitlick, and W. M. Lewis Jr. (2007), Use of Shields stress to reconstruct and forecast changes in river metabolism, *Freshwater Biol.*, *52*(8), 1587–1601, doi:10.1111/j.1365-2427.2007.01790.x.

Crowder, D. W., and P. Diplas (1997), Sampling heterogeneous deposits in gravel-bed streams, *J. Hydraul. Eng.*, *123*(12), 1106–1117, doi:10.1061/(ASCE)0733-9429(1997)123:12(1106).

Dietrich, W. E., P. A. Nelson, E. Yager, J. G. Venditti, M. P. Lamb, and L. Collins (2006), Sediment patches, sediment supply, and channel morphology, in *River, Coastal and Estuarine Morphodynamics: RCEM 2005*, vol. 1, edited by G. Parker and M. H. Garcia, pp. 79–90, A. A. Balkema, Leiden, Netherlands.

Fellows, C., H. Valett, C. Dahm, P. Mulholland, and S. Thomas (2006), Coupling nutrient uptake and energy flow in headwater streams, *Ecosystems*, *9*(5), 788–804.

Folke, C., S. Carpenter, B. Walker, M. Scheffer, T. Elmqvist, L. Gunderson, and C. S. Holling (2004), Regime shifts, resilience, and biodiversity in ecosystem management, *Annu. Rev. Ecol. Evol. Syst.*, *35*, 557–581, doi:10.1146/annurev.ecolsys.35.021103.105711.

Frankforter, J. D., H. S. Weyers, J. D. Bales, P. W. Moran, and D. L. Calhoun (2010), The relative influence of nutrients and habitat on stream metabolism in agricultural streams, *Environ. Monit. Assess.*, *168*, 461–479, doi:10.1007/s10661-009-1127-y.

Giller, P. S., and B. Malmqvist (2002), *The Biology of Streams and Rivers*, Oxford Univ. Press, Oxford, U. K.

Harvey, J. W., G. B. Noe, L. G. Larsen, D. J. Nowacki, and L. E. McPhillips (2011), Field flume reveals aquatic vegetation's role in sediment and particulate phosphorus transport in a shallow aquatic ecosystem, *Geomorphology*, *126*, 297–313.

Houser, J. N., P. J. Mulholland, and K. O. Maloney (2005), Catchment disturbance and stream metabolism: Patterns in ecosystem respiration and gross primary production along a gradient of upland soil and vegetation disturbance, *J. N. Am. Benthol. Soc.*, *24*(3), 538–552.

Izagirre, O., U. Agirre, M. Bermejo, J. Pozo, and A. Elosegi (2008), Environmental controls of whole-stream metabolism identified from continuous monitoring of Basque streams, *J. N. Am. Benthol. Soc.*, *27*(2), 252–268, doi:10.1899/07-022.1.

Junk, W. J., P. B. Bayley, and R. E. Sparks (1989), The flood pulse concept in river-floodplain systems, in *Proceedings of the International Large River Symposium*, edited by D. P. Dodge, *Can. Spec. Publ. Fish. Aquat. Sci.*, *106*, 110–127.

Kalkhoff, S. J., K. K. Barnes, K. D. Becher, M. E. Savoca, D. J. Schnoebelen, E. M. Sadorf, S. D. Porter, and D. J. Sullivan (2000), Water quality in the eastern Iowa basins, Iowa and Minnesota, 1996–98, *U.S. Geol. Surv. Circ.*, *1210*,

Karlen, D. L., M. D. Tomer, J. Neppel, and C. A. Cambardella (2008), A preliminary watershed scale soil quality assessment in north central Iowa, USA, *Soil Tillage Res.*, *99*(2), 291–299, doi:10.1016/j.still.2008.03.002.

Landon, M. K., D. L. Rus, and F. E. Harvey (2001), Comparison of instream methods for measuring hydraulic conductivity in sandy streambeds, *Ground Water*, *39*(6), 870–885.

Latulippe, C., M. F. LaPointe, and T. Talbot (2001), Visual characterization technique for gravel-cobble river bed surface sediments: Validation and environmental applications contribution to the Programme of Cirsa (Centre Interuniversaitaire de Recherche Sur le Saumon Atlantique), *Earth Surf. Processes Landforms*, *26*, 307–318, doi:10.1002/1096-9837(200103)26:3<307::AID-ESP160>3.0.CO;2-R.

Marzolf, E., P. Mulholland, and A. Steinman (1994), Improvements to the diurnal upstream-downstream dissolved oxygen change technique for determining whole-stream metabolism in small streams, *Can. J. Fish. Aquat. Sci.*, *51*(7), 1591–1599.

McDonald, R., J. Nelson, V. Paragamian, and G. Barton (2010), Modeling the effect of flow and sediment transport on White Sturgeon spawning habitat in the Kootenai River, Idaho, *J. Hydraul. Eng.*, *136*(12), 1077–1092, doi:10.1061/(ASCE)HY.1943-7900.0000283.

Moog, D. G., and G. H. Jirka (1998), Analysis of reaeration equations using mean multiplicative error, *J. Environ. Eng.*, *124*(2), 104–110.

Morgan, A. M., T. V. Royer, M. B. David, and L. E. Gentry (2006), Relationships among nutrients, chlorophyll-a, and dissolved oxygen in agricultural streams in Illinois, *J. Environ. Qual.*, *35*, 1110–1117, doi:10.2134/jeq2005.0433.

Mulholland, P., et al. (2001), Inter-biome comparison of factors controlling stream metabolism, *Freshwater Biol.*, *46*(11), 1503–1517, doi:10.1046/j.1365-2427.2001.00773.x.

Mulholland, P. J., J. N. Houser, and K. O. Maloney (2005), Stream diurnal dissolved oxygen profiles as indicators of in-stream metabolism and disturbance effects: Fort Benning as a case study, *Ecol. Indic.*, *5*(3), 243–252, doi:10.1016/j.ecolind.2005.03.004.

Munn, M., J. Frey, and A. Tesoriero (2010), The influence of nutrients and physical habitat in regulating algal biomass in agricultural streams, *Environ. Manage.*, *45*, 603–615, doi:10.1007/s00267-010-9435-0.

Nelson, J. M., J. P. Bennett, and S. M. Wiele (2003), Flow and sediment-transport modeling, in *Tools in Fluvial Geomorphology*, edited by G. M. Kondolf and H. Piégay, chap. 18, pp. 539–576, John Wiley, West Sussex, U. K.

Nelson, P. A., J. G. Venditti, W. E. Dietrich, J. W. Kichner, H. Ikeda, F. Iseya, and L. S. Sklar (2009), Response of bed surface patchiness to reductions in sediment supply, *J. Geophys. Res.*, *114*, F02005, doi:10.1029/2008JF001144.

O'Connor, B. L., and J. W. Harvey (2008), Scaling hyporheic exchange and its influence on biogeochemical reactions in aquatic ecosystems, *Water Resour. Res.*, *44*, W12423, doi:10.1029/2008WR007160.

O'Connor, B. L., and M. Hondzo (2008), Enhancement and inhibition of denitrification by fluid-flow and dissolved oxygen flux to stream sediments, *Environ. Sci. Technol.*, *42*(1), 119–125, doi:10.1021/es071173s.

Odum, H. T. (1956), Primary production in flowing waters, *Limnol. Oceanogr.*, *1*(2), 102–117.

Ogdahl, M. E., V. L. Lougheed, R. J. Stevenson, and A. D. Steinman (2010), Influences of multi-scale habitat on metabolism in a coastal Great Lakes watershed, *Ecosystems*, *13*(2), 222–238, doi:10.1007/s10021-009-9312-y.

Olden, J., and N. Poff (2003), Redundancy and the choice of hydrologic indices for characterizing streamflow regimes, *River Res. Applic.*, *19*(2), 101–121, doi:10.1002/rra.700.

Paola, C., and R. Seal (1995), Grain size patchiness as a cause of selective deposition and downstream fining, *Water Resour. Res.*, *31*(5), 1395–1407.

Schnoebelen, D. J., S. J. Kalkhoff, K. D. Becher, and E. Thurman (2003), Water-quality assessment of the eastern Iowa basins: Selected pesticides and pesticide degradates in streams, 1996–98, *U.S. Geol. Surv. Water Resour. Invest. Rep.*, *03-4075*.

Singer, G., K. Besemer, P. Schmitt-Kopplin, I. Hödl, and T. J. Battin (2010), Physical heterogeneity increases biofilm resource use and its molecular diversity in stream mesocosms, *PLoS ONE*, *5*(4), e9988, doi:10.1371/journal.pone.0009988.

Sorenson, S. K., S. D. Porter, K. K. B. Akers, M. A. Harris, S. J. Kalkhoff, K. E. Lee, L. R. Roberts, and P. J. Terrio (1999), Water quality and habitat conditions in upper Midwest streams relative to riparian vegetation and soil characteristics, August 1997: Study Design, Methods, and Data, *U.S. Geol. Surv. Open File Rep.*, *99-202*.

Tomer, M., T. Moorman, and C. Rossi (2008), Assessment of the Iowa River's South Fork watershed: Part 1. Water quality, *J. Soil Water Conserv.*, *63*(6), 360–370.

Turnipseed, D. P., and V. B. Sauer (2010), Discharge measurements at gaging stations, in *U.S. Geol. Surv. Tech. Methods*, Book 3, Chapter A8, 106 pp.

Uehlinger, U. (2000), Resistance and resilience of ecosystem metabolism in a flood-prone river system, *Freshwater Biol.*, *45*(3), 319–332, doi:10.1046/j.1365-2427.2000.00620.x.

Uehlinger, U. (2006), Annual cycle and inter-annual variability of gross primary production and ecosystem respiration in a floodprone river during a 15-year period, *Freshwater Biol.*, *51*(5), 938–950, doi:10.1111/j.1365-2427.2006.01551.x.

Uehlinger, U., and M. W. Naegeli (1998), Ecosystem metabolism, disturbance, and stability in a prealpine gravel bed river, *J. N. Am. Benthol. Soc.*, *17*(2), 165–178.

Vericat, D., R. J. Batalla, and C. N. Gibbins (2008), Sediment entrainment and depletion from patches of fine material in a gravel-bed river, *Water Resour. Res.*, *44*, W11415, doi:10.1029/2008WR007028.

Warnaars, T. A., M. Hondzo, and M. E. Power (2007), Abiotic controls on periphyton accrual and metabolism in streams: Scaling by dimensionless numbers, *Water Resour. Res.*, *43*, W08425, doi:10.1029/2006WR005002.

Whiting, P. J., W. E. Dietrich, L. B. Leopold, T. G. Drake, and R. L. Shreve (1988), Bedload sheets in heterogeneous sediment, *Geology*, *16*(2), 105–108.

Wilcock, P. R., and B. T. DeTemple (2005), Persistence of armor layers in gravel-bed streams, *Geophys. Res. Lett.*, *32*, L08402, doi:10.1029/2004GL021772.

Wiley, M. J., L. L. Osborne, and R. W. Larimore (1990), Longitudinal structure of an agricultural prairie river system and it relationship to current stream ecosystem theory, *Can. J. Fish. Aquat. Sci.*, *47*, 373–384.

Wilson, K. C., and W. K. Dodds (2009), Centimeter-scale stream substratum heterogeneity and metabolic rates, *Hydrobiologia*, *623*(1), 53–62, doi:10.1007/s10750-008-9647-y.

Wong, M., and G. Parker (2006), Reanalysis and correction of bed-load relation of Meyer-Peter and Müller using their own database, *J. Hydraul. Eng.*, *132*(11), 1159–1168, doi:10.1061/(ASCE)0733-9429(2006)132:11(1159).

Young, R. G., and A. D. Huryn (1996), Interannual variation in discharge controls ecosystem metabolism along a grassland river continuum, *Can. J. Fish. Aquat. Sci.*, *53*, 2199–2211.

Young, R. G., and A. D. Huryn (1999), Effects of land use on stream metabolism and organic matter turnover, *Ecol. Appl.*, *9*, 1359–1376.